International Journal of Nanoelectronics and Materials
In Press, Accepted Manuscript – Note to user

Prediction Effects on Internal Resonance Wave of Metallic Conductive Ink in Rotational Motion Behaviour

Mohd Azli Salim[1,2,*], Feng Dai[3], Adzni Md. Saad[2], Nor Azmmi Masripan[2], Andrey Nikolayevich Dmitriev[4], Azmi Naroh[5], Ghazali Omar[1,2] and Mohd Zaid Akop[2]

[1]Advanced Manufacturing Centre, Universiti Teknikal Malaysia Melaka, Hang Tuah Jaya, 76100 Durian Tunggal, Melaka, Malaysia.
[2]Fakulti Kejuruteraan Mekanikal, Universiti Teknikal Malaysia Melaka, Hang Tuah Jaya, 76100 Durian Tunggal, Melaka, Malaysia.
[3]China Railway Eryuan Engineering Group Co., Ltd, No. 3 Tongjin Road, Chengdu, China.
[4]Institute of Metallurgy of Ural Branch of Russian Academy of Sciences, Ural Federal University, Russia.
[5]Jabatan Kejuruteraan Mekanikal, Politeknik Ungku Omar, Jalan Raja Musa Mahadi, 31400 Ipoh, Perak, Malaysia.

ABSTRACT

This paper represents the effects on internal resonance wave of metallic conductive ink in rotational motion behaviour. The internal resonance metallic conductive ink model is developed using wave propagation approach. There are two equations are derived which are impedance and stiffness. Based on these two equations, the multi-body of metallic conductive ink model has been successfully derived in order to observe the behaviour of internal resonance, when force applied at the both end of the model. The internal resonance wave was predicted, and the results have been recorded, and finally, the location of the internal resonance has been identified. The maximum level of frequency has recorded at 10 kHz. This results are believed can be used in future analysis of metallic conductive ink in order to evaluate and investigate the range of the conductivity of the ink with predictive method.

Keywords: conductive ink, internal resonance, rotational behavior

1. INTRODUCTION

Recently, many of electronic product were made from micron-size [1]. It happens because of the progressive advancement of future technology to replace the current electronic packaging, rigid electronic and super scale packaging. Therefore, the revolution of micron-size technology is needed for tomorrow technology [2-3].

Metallic conductive ink (MCI) has a capable to produce electrical conductivity in small value. Many conductive ink has been made by metal materials because the materials itself has high conductivity coefficients. In addition, the ink capable to expand, and it is allowed many applications to use it as a secondary circuit to operate the system [4]. However, until today, the level of conductivity of the ink only can be investigated and evaluated using experimental approach [5]. Based on this approach, many efforts and finance have been used by engineers and researchers [6-7].

In this paper, the MCI model was developed using modelling estimation and prediction approach for non-linear technique. In this study, the model was represented as a baseline MCI model with conductivity range. The conductivity material basically has been blend together with polymer in order to have a one shape. This prediction technique will be used in order to check and examine the range of conductivity of the MCI model.

Note: Accepted manuscripts are articles that have been peer-reviewed and accepted for publication by the Editorial Board. These articles have not yet been copyedited and/or formatted in the journal house style.

2. MATERIAL AND METHODS

Consider a uniform stretchable conductive ink (SCI) model having L length subjected to a longitudinal direction of force as shown in Figure 1.

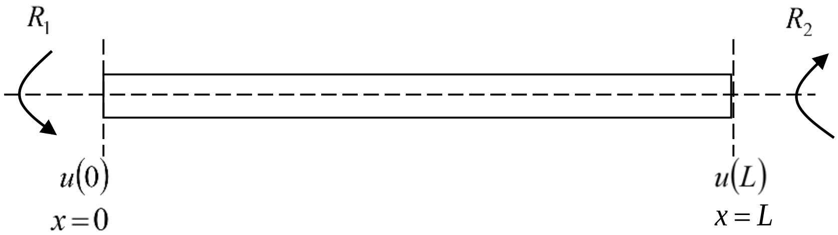

Figure 1. The uniform stretchable conductive ink model having *L* length subjected to a longitudinal direction of force.

The general equation of motion for the SCI model can be represented as

$$c_r^2 \frac{\partial^2 u(x,t)}{\partial^2 x} = \frac{\partial^2 u(x,t)}{\partial^2 t} \quad (1)$$

where $c_r = \sqrt{G/\rho}$ and G is complex shear modulus and ρ is density.

By applying the forces at the both end of the SCI model, it generates the harmonic reaction and Eq. (1) produces negative and positive going wave in the microstructure reaction, and it can be represented in Figure 2 and the new equation illustrates in Eq. (2).

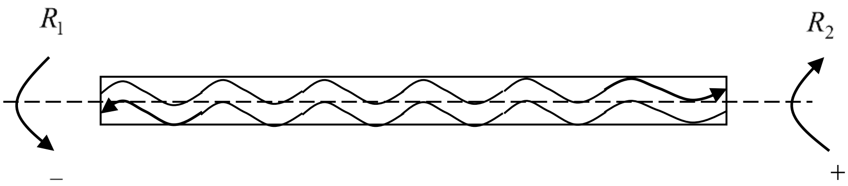

Figure 2. Forces applying at the both end of stretchable conductive ink model and it produces negative and positive going wave in microstructure reaction

$$u(x,t) = u(x)e^{j\omega t} = \left(A_r e^{jk_r x} + B_r e^{-jk_r x}\right)e^{j\omega t} \quad (2)$$

where A_r and B_r are complex wave amplitudes.

For rotational of SCI model, shear wavenumber equation can be represented as

$$k_r = \frac{\omega}{c_r} = \sqrt{\frac{\rho}{G}} \cdot \omega \quad (3)$$

At point impedance, it said that the SCI model at each end are equal due to symmetry. Based on this theoretically understanding, it becomes

$$Z_{11} = \left.\frac{R_1}{\dot{u}(0)}\right|_{\dot{u}(L)=0}$$

and

$$Z_{22}=\left.\frac{R_2}{\dot{u}(L)}\right|_{\dot{u}(0)=0} \tag{4}$$

By applying Hooke Law at $x=0$, the previous equation can be written as

$$jk_rA_r=jk_rB_r=-\frac{R_1}{\kappa_r}$$

and

$$A_r-B_r=-\frac{R_1}{\kappa_r\,jk_r} \tag{5}$$

According to Eq. (5), the new equation can be given as

$$\frac{\partial u(0)}{\partial x}=-\frac{R_1}{\kappa_r} \tag{6}$$

where $\kappa_r=G\cdot J_r$, J_r is polar second moment of area of SCI model based on rectangular shape.

At boundary condition $x=L$, the equation become

$$\dot{u}(L)=j\omega u(L)=0 \tag{7}$$

By substituting Eq. (2) into Eq. (6) and Eq. (7), and the letting the boundary condition at $x=0$ and $x=L$, Eq. (6) can be rearranged as

$$A_r\left(1+e^{2jk_rL}\right)=-\frac{R_1}{\kappa_r\,jk_r} \tag{8}$$

Then, it is followed by Eq. (7),

$$A_re^{jk_rL}+B_re^{-jk_rL}=0 \tag{9}$$

By simplify Eq. (9), the equation is become

$$A_re^{2jk_rL}+B_r=0 \tag{10}$$

Finally, the equations are become

$$A_r=-\frac{R_1}{jk_r\kappa_r}\cdot\frac{1}{e^{2jk_rL}+1}$$

and

$$B_r = \frac{R_1}{jk_r\kappa_r} \cdot \frac{e^{2jk_rL}}{e^{2jk_rL}+1} \tag{11}$$

By substituting Eq. (11) into Eq. (2) and letting boundary condition at $x = 0$, so

$$u(0) = \frac{R_1}{jk_r\kappa_r} \cdot \frac{e^{2jk_rL}-1}{e^{2jk_rL}+1} = \frac{R_1}{k_r\kappa_r} \cdot \tan(k_rL) \tag{12}$$

From Eq. (12), differentiate the equation into time and it gives

$$Z_{11} = \frac{R_1}{\dot{u}(0)} = \frac{R_1}{j\omega u(0)} = \frac{k_r\kappa_r}{j\omega \tan(k_rL)} \tag{13}$$

For transfer impedance, it said that the SCI model at each end are equal to reciprocity [8 -9]. According to this statement, the impedance equation become

$$Z_{12} = \left.\frac{R_1}{\dot{u}(L)}\right|_{\dot{u}(0)=0}$$

and

$$Z_{21} = \left.\frac{R_2}{\dot{u}(0)}\right|_{\dot{u}(L)=0} \tag{14}$$

For $x = 0$ and by applying Hooke Law again, it is still valid. Then, for Z_{12} is it become

$$\dot{u}(0) = j\omega u(0) = 0 \tag{15}$$

By substituting Eq. (2) into Eq. (6) and Eq. (15) by letting boundary condition at $x = 0$, the new equation is become

$$A = -\frac{R_1}{2jk_r\kappa_r}$$

and

$$B = \frac{R_1}{2jk_r\kappa_r} \tag{16}$$

Insert Eq. (16) into Eq. (2) and letting boundary condition at $x = L$, the equation is become

$$u(L) = \frac{R_1}{2jk_r\kappa_r} \cdot \left(e^{-jk_rL} - e^{jk_rL}\right) = -\frac{R_1}{k_r\kappa_r} \cdot \sin(k_rL) \tag{17}$$

Take Eq. (17) and differentiate respect to time and the new equation is become

$$Z_{12} = \frac{R_1}{\dot{u}(L)} = \frac{R_1}{j\omega u(L)} = -\frac{k_r \kappa_r}{j\omega \sin(k_r L)} \tag{18}$$

The impedance matrix SCI model matrix is

$$Z = \begin{bmatrix} Z_{11} & Z_{12} \\ Z_{21} & Z_{22} \end{bmatrix} = \frac{k_r \kappa_r}{j\omega \sin(k_r L)} \cdot \begin{bmatrix} \cos(k_r L) & -1 \\ -1 & \cos(k_r L) \end{bmatrix} \tag{19}$$

By substituting k_r and κ_r for rotational internal resonance of SCI model, the equation is become

$$Z = \begin{bmatrix} Z_{11} & Z_{12} \\ Z_{21} & Z_{22} \end{bmatrix} = \frac{J_r \sqrt{G \cdot \rho}}{j \sin(k_r L)} \cdot \begin{bmatrix} \cos(k_r L) & -1 \\ -1 & \cos(k_r L) \end{bmatrix} \tag{20}$$

By simplifying Eq. (20),

$$Z_{11} = \frac{J_r \sqrt{G \cdot \rho}}{j \sin(k_r L)} \cdot \cos(k_s L) = \frac{J_r \sqrt{G \cdot \rho} \cdot \cos(k_r L)}{j \sin(k_r L)} = -jJ_r \sqrt{G \cdot \rho} \cdot \cot(k_r L) \tag{21}$$

$$Z_{12} = \frac{J_r \sqrt{G \cdot \rho}}{j \sin(k_r L)} \cdot -1 = \frac{jJ_r \sqrt{G \cdot \rho}}{\sin(k_r L)} \tag{22}$$

$$Z_{21} = \frac{J_r \sqrt{G \cdot \rho}}{j \sin(k_r L)} \cdot -1 = \frac{jJ_r \sqrt{G \cdot \rho}}{\sin(k_r L)} \tag{23}$$

and

$$Z_{22} = \frac{J_r \sqrt{G \cdot \rho}}{j \sin(k_r L)} \cdot \cos(k_r L) = \frac{J_r \sqrt{G \cdot \rho} \cdot \cos(k_r L)}{j \sin(k_r L)} = -jJ_r \sqrt{G \cdot \rho} \cdot \cot(k_r L) \tag{24}$$

In matrix form for impedance of SCI model can be written as

$$Z = \begin{bmatrix} Z_{11} & Z_{12} \\ Z_{21} & Z_{22} \end{bmatrix} = \begin{bmatrix} -jJ_r \sqrt{G \cdot \rho} \cdot \cot(k_r L) & \dfrac{jJ_r \sqrt{G \cdot \rho}}{\sin(k_r L)} \\ \dfrac{jJ_r \sqrt{G \cdot \rho}}{\sin(k_r L)} & -jJ_r \sqrt{G \cdot \rho} \cdot \cot(k_r L) \end{bmatrix} \tag{25}$$

Finally, the relationship between the equations in Eq. (21) to Eq. (24) can be simplified as below.

$$Z_{11} = Z_{22} = -jJ_r \sqrt{G \cdot \rho} \cdot \cot(k_r L)$$

and

$$Z_{12} = Z_{21} = \frac{jJ_r \sqrt{G \cdot \rho}}{\sin(k_r L)} \tag{26}$$

Impedance equation also can be written in stiffness domain for SCI model. In stiffness, the equation become

$$K_{11} = K_{22} = \frac{R_1}{X_1} = \frac{GA}{h}\left(\frac{k_r h}{\tan(k_r h)}\right)$$

and

$$K_{12} = K_{21} = \frac{R_2}{X_1} = \frac{GA}{h}\left(\frac{k_r h}{\sin(k_r h)}\right) \quad (27)$$

where h is the thickness of the sample and A is a cross sectional area for hybrid vibration control model.

According to Eq. (27), it only can be used for a singular body. In multi-body system, both equations need to be arranged and matrix form is used. In singular body, the equation shown in Eq. (28).

$$\text{One DOF for SCI model } = \begin{bmatrix} \overset{(1)}{K}_{(11)} & \overset{(1)}{K}_{(12)} \\ \overset{(1)}{K}_{(21)} & \overset{(1)}{K}_{(22)} \end{bmatrix} \quad (28)$$

where $\overset{(1)}{K}_{11}$ referred to the stiffness for element 1 at coordinate (1,1), $\overset{(1)}{K}_{12}$ referred to the stiffness for element 1 at coordinate (1,2), $\overset{(1)}{K}_{21}$ referred to the stiffness for element 1 at coordinate (2,1) and $\overset{(1)}{K}_{22}$ referred to the stiffness for element 1 at coordinate (2,2).

The coordinate can be plotted at uniform SCI model and shown in Figure 3.

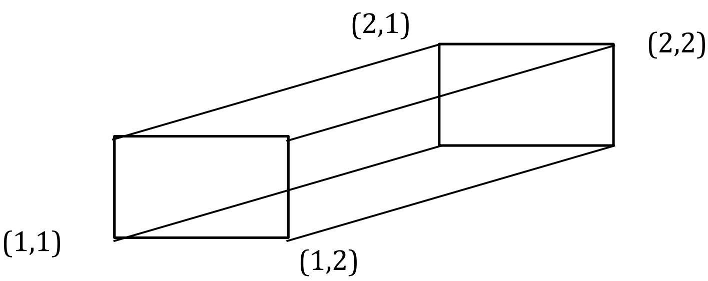

Figure 3. Coordinate for stretchable conductive ink model.

Based on the figure, the multi-body system for SCI model, can be written in matrix form. Additionally, the two, three and four bodies of hybrid control vibration system equation can be represented as

Two bodies for SCI model $= \begin{bmatrix} \overset{(1)}{K}_{(11)} & \overset{(1)}{K}_{(12)} \\ \overset{(1)}{K}_{(21)} & \overset{(1)}{K}_{(22)} \end{bmatrix} + \begin{bmatrix} \overset{(2)}{K}_{(11)} & \overset{(2)}{K}_{(12)} \\ \overset{(2)}{K}_{(21)} & \overset{(2)}{K}_{(22)} \end{bmatrix} = \begin{bmatrix} \overset{(1)}{K}_{(11)} + \overset{(2)}{K}_{(11)} & \overset{(1)}{K}_{(12)} + \overset{(2)}{K}_{(12)} \\ \overset{(1)}{K}_{(21)} + \overset{(2)}{K}_{(21)} & \overset{(1)}{K}_{(22)} + \overset{(2)}{K}_{(22)} \end{bmatrix}$ (29)

Three bodies for SCI model

$$= \begin{bmatrix} \overset{(1)}{K}_{(11)} & \overset{(1)}{K}_{(12)} \\ \overset{(1)}{K}_{(21)} & \overset{(1)}{K}_{(22)} \end{bmatrix} + \begin{bmatrix} \overset{(2)}{K}_{(11)} & \overset{(2)}{K}_{(12)} \\ \overset{(2)}{K}_{(21)} & \overset{(2)}{K}_{(22)} \end{bmatrix} + \begin{bmatrix} \overset{(3)}{K}_{(11)} & \overset{(3)}{K}_{(12)} \\ \overset{(3)}{K}_{(21)} & \overset{(3)}{K}_{(22)} \end{bmatrix} = \begin{bmatrix} \overset{(1)}{K}_{(11)} + \overset{(2)}{K}_{(11)} + \overset{(3)}{K}_{(11)} & \overset{(1)}{K}_{(12)} + \overset{(2)}{K}_{(12)} + \overset{(3)}{K}_{(12)} \\ \overset{(1)}{K}_{(21)} + \overset{(2)}{K}_{(21)} + \overset{(3)}{K}_{(21)} & \overset{(1)}{K}_{(22)} + \overset{(2)}{K}_{(22)} + \overset{(3)}{K}_{(22)} \end{bmatrix} \tag{30}$$

Four bodies for SCI model

$$= \begin{bmatrix} \overset{(1)}{K}_{(11)} & \overset{(1)}{K}_{(12)} \\ \overset{(1)}{K}_{(21)} & \overset{(1)}{K}_{(22)} \end{bmatrix} + \begin{bmatrix} \overset{(2)}{K}_{(11)} & \overset{(2)}{K}_{(12)} \\ \overset{(2)}{K}_{(21)} & \overset{(2)}{K}_{(22)} \end{bmatrix} + \begin{bmatrix} \overset{(3)}{K}_{(11)} & \overset{(3)}{K}_{(12)} \\ \overset{(3)}{K}_{(21)} & \overset{(3)}{K}_{(22)} \end{bmatrix}. + \begin{bmatrix} \overset{(4)}{K}_{(11)} & \overset{(4)}{K}_{(12)} \\ \overset{(4)}{K}_{(21)} & \overset{(4)}{K}_{(22)} \end{bmatrix} \ldots$$

(31)

$$\ldots = \begin{bmatrix} \overset{(1)}{K}_{(11)} + \overset{(2)}{K}_{(11)} + \overset{(3)}{K}_{(11)} + \overset{(4)}{K}_{(11)} & \overset{(1)}{K}_{(12)} + \overset{(2)}{K}_{(12)} + \overset{(3)}{K}_{(12)} + \overset{(4)}{K}_{(12)} \\ \overset{(1)}{K}_{(21)} + \overset{(2)}{K}_{(21)} + \overset{(3)}{K}_{(21)} + \overset{(4)}{K}_{(21)} & \overset{(1)}{K}_{(22)} + \overset{(2)}{K}_{(22)} + \overset{(3)}{K}_{(22)} + \overset{(4)}{K}_{(22)} \end{bmatrix}$$

By following the pattern from Eq. (29) to Eq. (31), the multi-body matrix for SCI model can be derived as

Multi-body of SCI model

$$= \begin{bmatrix} \overset{(n-(n-1))}{K}_{(11)} & \overset{(n-(n-1))}{K}_{(12)} \\ \overset{(n-(n-1))}{K}_{(21)} & \overset{(n-(n-1))}{K}_{(22)} \end{bmatrix} + \begin{bmatrix} \overset{(n-(n-2))}{K}_{(11)} & \overset{(n-(n-2))}{K}_{(12)} \\ \overset{(n-(n-2))}{K}_{(21)} & \overset{(n-(n-2))}{K}_{(22)} \end{bmatrix} + \begin{bmatrix} \overset{(n-(n-3))}{K}_{(11)} & \overset{(n-(n-3))}{K}_{(12)} \\ \overset{(n-(n-3))}{K}_{(21)} & \overset{(n-(n-3))}{K}_{(22)} \end{bmatrix} + \begin{bmatrix} \overset{(n-(n-n))}{K}_{(11)} & \overset{(n-(n-n))}{K}_{(12)} \\ \overset{(n-(n-n))}{K}_{(21)} & \overset{(n-(n-n))}{K}_{(22)} \end{bmatrix} \tag{32}$$

where n is the maximum number of bodies.

Equation (32) can be illustrated in the diagram with the length of the system is constants but divided into small parts. By doing this, the same system is presumed transferred to multi-body of SCI model. Figure 4 show the multi-body diagram for SCI model.

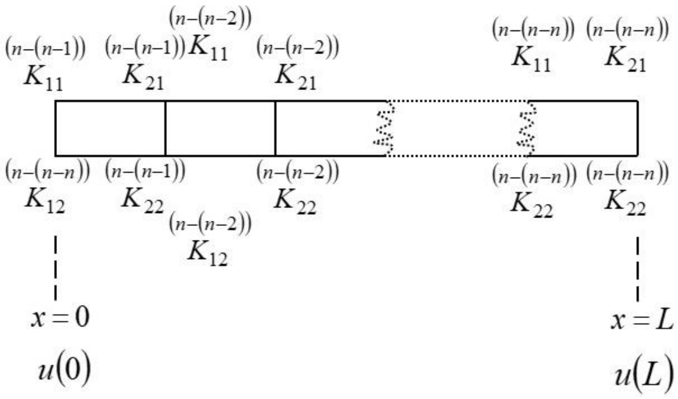

Figure 4. Multi-body diagram for SCI model.

3. RESULTS AND DISCUSSION

Internal resonance wave effects are based on many factors which depend on the materials shape, properties, radius, length, thickness and the most importantly is boundary condition of the materials during tests. All of these factors give effect in term of deformation, shear, compression, elongation and many more. Wave effects are more important for stretchable and flexible materials because the static stiffness is bigger than the rigid and non-flexible materials.
Wave effects also can exchange the energy between conventional motions is a same or different direction. It is occurred when the different motions in different directions was interrupted the dynamic behavior and mostly affect the internal strengthen of the materials, and in this study, it will affect the conductivity of the metallic materials itself. The internal resonances are produced by two methods which are impedance and stiffness.

In impedance, there have for internal resonances location detected at the longitudinal wave direction of SCI model. Based on these four locations, the internal resonance of SCI model is occurred when the frequency reached at 1 kHz and above. At these frequencies range, internal wave was generated from applying tension force and then, it fluctuated at the end of the SCI model and called as positive wave. After reaching at the end, the direction of internal wave has changed and goes back to the initial boundary and called as negative wave feedback.

All of the result shown in Figure 5. In addition, internal resonance of SCI model also can be plotted in stiffness and the results shown in Figure 6.

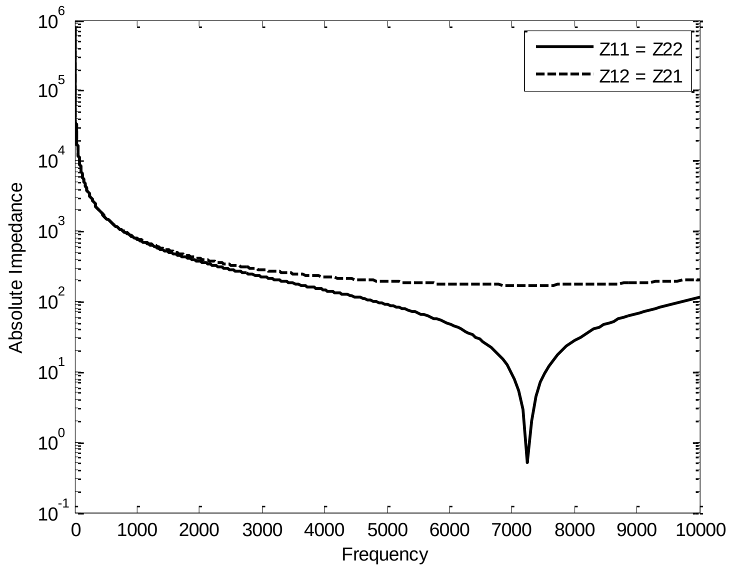

Figure 5. Impedance for stretchable conductive ink model.

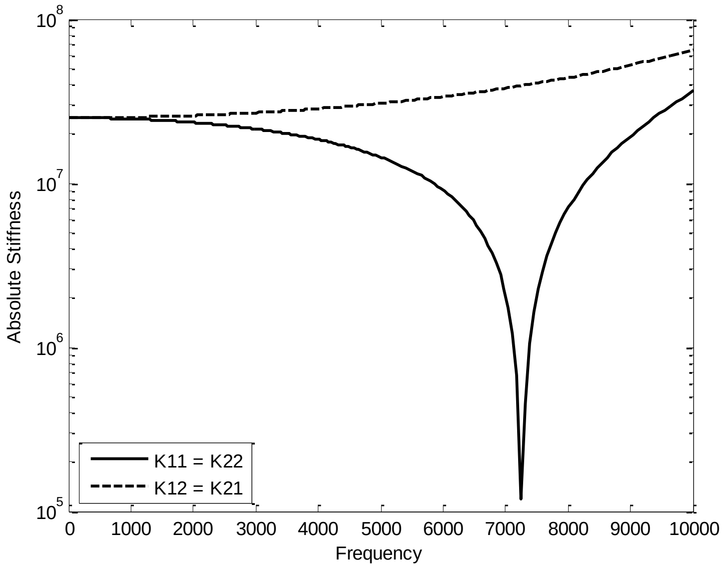

Figure 6. Stiffness for stretchable conductive ink model.

4. CONCLUSION

This study represents the modelling estimation and prediction of SCI model due to internal resonance wave effect. There are two types of dynamic formulation, which are impedance and stiffness. The multi-body of SCI model has been successfully developing, and based on the results, the internal resonance for SCI models occurred at same point and it was recorded until 10 kHz. One conclusion has been observed, this effects can be used to investigate and evaluate the conductivity performance of metallic based materials in electronic packaging industry in future.

ACKNOWLEDGEMENTS

This work partially supported by the grant PJP/2016/FKM-CARE/S01506 of Universiti Teknikal Malaysia Melaka (UTeM). Gratitude also expressed to Advanced Manufacturing Centre and Fakulti Kejuruteraan Mekanikal, UTeM.

REFERENCES

[1] Li, Tianhua, and Hongbo Hu. Preparation and Performance of Conductive Copper Ink Based on Chemical Deoxidization. Chemical Engineering Transactions, issue **66** (2018) pp. 31-36.

[2] Titkov, A. I., O. G. Bukhanets, R. M. Gadirov, Yu M. Yukhin, and N. Z. Lyakhov. Conductive inks for inkjet printing based on composition of nanoparticles and organic silver salt. Inorganic Materials: Applied Research, issue **6**, no. 4 (2015) pp. 375-381.

[3] Sergeev, A. S., A. R. Tameev, V. I. Zolotarevskii, and A. V. Vannikov. Electrically conductive inks based on polymer composition for inkjet printing. Inorganic Materials: Applied Research, issue **9**, no. 1 (2018) pp. 147-150.

[4] Salim, Mohd Azli., Roshidah Hamidi, and Adzni Md Saad. Development of Sheet Resistivity on Silver Nanoparticle Filled Epoxy for Electronic Packaging Devices. In 1st Colloquium Paper: Advanced Materials and Mechanical Engineering Research (CAMMER'18), vol. **1**. Penerbit Universiti, Universiti Teknikal Malaysia Melaka (2018) pp 1-5.

[5] Omar, G., M. A. Salim, B. R. Mizah, A. A. Kamarolzaman, and R. Nadlene. Electronic Applications of Functionalized Graphene Nanocomposites. In Functionalized Graphene Nanocomposites and their Derivatives. (2019) pp. 245-263.

[6] Rosszainily, I. R. A., Salim, M. A., Mansor, M. R., Akop, M. Z., Putra, A., Musthafah, M. T., & Sudin, M. N. Effect of carbon black fillers on tensile stress of unvulcanized natural rubber compound. Journal of Mechanical Engineering and Sciences, issue **10,** no. 2 (2016) pp. 2043-2052.

[7] Salim, M. A., Putra, A., & Abdullah, M. A. Analysis of axial vibration in the laminated rubber-metal spring. In Advanced Materials Research, issue **845** (2014) pp. 46-50.

[8] Abbasi, Amirhassan, S. E. Khadem, and Saeed Bab, Vibration control of a continuous rotating shaft employing high-static low-dynamic stiffness isolators. Journal of Vibration and Control, issue **24**. no. 4 (2018) pp. 760-783.

[9] Nguyen, X. B., Komatsuzaki, T., Iwata, Y., & Asanuma, H. Modeling and semi-active fuzzy control of magnetorheological elastomer-based isolator for seismic response reduction. Mechanical Systems and Signal Processing, issue **101** (2018) pp. 449-466.